Structure-based discovery of positive allosteric modulators for the calcium sensing receptor

Fangyu Liu[1,†], Cheng-Guo Wu[2,†], Chia-Ling Tu[3], Isabella Glenn[1], Justin Meyerowitz[2,], Anat Levit Kaplan[1], Jiankun Lyu[1,4], Zhiqiang Cheng[3], Olga O. Tarkhanova[5], Yurii S. Moroz[5,6,7], John J. Irwin[1], Wenhan Chang[3,*], Brian K. Shoichet[1,*] & Georgios Skiniotis[*,2,8].

[†] Contributed equally.

* Corresponding authors: Wenhan.Chang@ucsf.edu, shoichet@cgl.ucsf.edu, yiorgo@stanford.edu

Affiliations:

1. Dept. of Pharmaceutical Chemistry, University of California, San Francisco, San Francisco CA 94143, USA.
2. Department of Molecular and Cellular Physiology, Stanford University School of Medicine, Stanford, CA, USA
3. San Francisco VA Medical Center, Dept. of Medicine, University of California, San Francisco, San Francisco CA 94158, USA.
4. Current address: The Rockefeller University, New York, NY, 10065
5. Chemspace LLC, Kyiv, 02094, Ukraine
6. Taras Shevchenko National University of Kyiv, Kyiv, 01601, Ukraine
7. Enamine Ltd., Kyiv, 02094, Ukraine
8. Department of Structural Biology, Stanford University School of Medicine, Stanford, CA, USA

`

Abstract

Drugs acting as positive allosteric modulators (PAMs) to enhance the activation of the calcium sensing receptor (CaSR) and to suppress parathyroid hormone (PTH) secretion can treat hyperparathyroidism but suffer from side effects including hypocalcemia and arrhythmias. Seeking new CaSR modulators, we docked libraries of 2.7 million and 1.2 billion molecules against transforming pockets in the active-state receptor dimer structure. Consistent with the idea that docking improves with library size, billion-molecule docking found new PAMs with a hit rate that was 2.7-fold higher than the million-molecule library and with hits up to 37-fold more potent. Structure-based optimization of ligands from both campaigns led to nanomolar leads, one of which was advanced to animal testing. This PAM displays 100-fold the potency of the standard of care, cinacalcet, in *ex vivo* organ assays, and reduces serum PTH levels in mice by up to 80% without the hypocalcemia typical of CaSR drugs. Cryo-EM structures with the new PAMs show that they promote CaSR dimer conformations that are closer to the G-protein coupled state compared to established drugs. These findings highlight the promise of large library docking for therapeutic leads, especially when combined with experimental structure determination and mechanism.

`

Introduction

Well before the advent of molecular pharmacology, much effort had been directed toward developing "calcimimetic" and "calcilytic" drugs to promote or suppress the calcium-sensing abilities of parathyroid cells and to regulate PTH secretion and blood calcium levels. The activity of these drugs on the calcium-sensing receptor (CaSR), a G protein-coupled receptor (GPCR), was confirmed after its cloning[1]. CaSR is present in almost every organ system but is most highly expressed in the parathyroid gland and in the kidneys, where it maintains calcium homeostasis by sensing changes in extracellular calcium levels to regulate PTH secretion, renal calcium reabsorption, and excretion[2,3]. Loss-of-function mutations or reduced CaSR expression cause familial hypocalciuric hypercalcemia (FHH), neonatal severe primary hyperparathyroidism, or adult primary hyperparathyroidism, respectively[4]. In FHH, the CaSR becomes less sensitive to rising calcium levels, leading to increased PTH secretion *in lieu* of elevated blood calcium levels and reduced calcium excretion. Conversely, oversensitivity to calcium from gain-of-function mutations in autosomal dominant hypocalcemia (ADH) decreases PTH secretion and lowers blood calcium levels[5-7]. Through its widespread expression, CaSR is also involved in other physiological mechanisms, notably gastrointestinal nutrient sensing, vascular tone, and secretion of insulin, with alterations in receptor activity implicated in the development of osteoporosis and in several cancers[3].

Efforts to target CaSR therapeutically have focused on the development of positive and negative allosteric modulators (PAMs and NAMs), which potentiate the receptor's activation or its inactivation, respectively, while binding at a non-orthosteric site (here, a non-calcium site). PAMs enhance the physiological response to calcium but display little or no agonist activity on their own. In the past two decades, the small molecule PAM drug cinacalcet and the peptide-based PAM drug etelcalcetide[8] were approved for human use, but only for the treatment of secondary hyperparathyroidism (HPT) in patients with chronic kidney disease (CKD) undergoing dialysis,

`

while cinacalcet is also approved to treat high levels of calcium in patients with parathyroid cancer. The limited indications reflect the adverse side effects associated with the current PAMs, including hypocalcemia, upper gastrointestinal bleeding, hypotension, and adynamic bone disease. Hypocalcemia can be life-threatening as it can cause seizures and heart failure[9-14], and thus drugs that decrease PTH levels without this adverse effect are much needed.

The CaSR belongs to the Family C of GPCRs, a relatively exotic group that has the unique property of operating as homo- or heterodimers with extracellular domains (ECDs) constituting the orthosteric ligand binding site. The ECD of a CaSR monomer is connected through a linker region to the seven transmembrane domain (7TM), which has been shown to activate primarily to Gq/11 and Gi/o G protein subtypes[15,16]. Upon calcium binding to the ECDs, the CaSR homodimer undergoes extensive conformational transitions that bring the 7TMs in close proximity with a TM6-TM6 interface, an overall configuration that has been shown to be associated with receptor coupling to G protein[17,18]. Our recent high resolution cryo-EM studies showed that in the active-state receptor both cinacalcet and the related evocalcet, recently approved for therapeutic use in Japan[16], both adopt an “extended” conformation within the 7TM of one CaSR monomer, and a “bent” conformation in the second monomer of the dimer. The two different conformations by the same ligand reflect changes in the allosteric PAM binding pockets that are transforming to accommodate the asymmetric juxtaposition of the two CaSR protomers upon activation[16].

We sought to exploit these structures and our mechanistic insights on receptor activation to discover new CaSR PAM chemotypes that are topologically unrelated to those previously investigated. Such new chemotypes often lead to new pharmacology, and our hope was that they might enhance CaSR activation and so modulate PTH secretion without leading to the dose-limiting hypocalcemic actions of approved drugs. To address this, we adopted a structure-based, library docking approach[19]. In the last four years, docking libraries have expanded over 1000-fold,

`

from millions to billions of molecules, and from these new libraries have emerged unusually potent ligands, with activities often in the mid- to low-nM concentration range, straight from docking[19-25]. Indeed, simulations suggest that as the libraries expand, docking finds not only more but better ligands, although this has not been experimentally tested. While our chief goal was the discovery of efficacious CaSR PAMs with reduced side-effects, we took the opportunity to test how library growth affected docking experimentally, comparing the *in vitro* results from docking a 2.7 million library vs. a library of 1.2 billion molecules. This offers one of the first experimental tests for the impact of library growth on experimental outcome. Mechanistically and therapeutically, potent new PAMs emerged from these studies, active in the 3 nM range, with *in vivo* activities between 10 and 100-fold more potent than cinacalcet, and apparently without that drug's dose-limiting hypocalcemia. Cryo-EM structures of the new PAMs illuminate their mechanism of action on CaSR and may template future optimization and discovery toward better therapeutics.

Results

Docking a small in-stock library against CaSR. We began by docking the smaller, in-stock library of 2.7 million molecules at both 7TM sites of CaSR. In the site accommodating the "bent" conformation of cinacalcet ($7TM^B$ site), an average of 3,927 orientations of each library ligand were sampled, each in an average of 333 conformations, or 1.2 trillion configurations overall; the calculation took just under one hour of elapsed time on a 1000-core cluster, using DOCK3.7[26]. Molecules were scored for van der Waals[27] and Poisson-Boltzmann-based electrostatic complementarity[28,29] corrected for Generalized-Born ligand desolvation[30]. Conformationally strained molecules were deprioritized[31], while high-ranking molecules were clustered for similarity to each other using an ECFP4-based Tanimoto coefficient (Tc) of 0.5 and filtered against similarity to known CaSR ligands. Comparable numbers of ligand orientations, conformations, and docking configurations were sampled and calculated for the "extended" site ($7TM^A$ site). Ultimately, we selected 26 compounds with favorable interactions at the $7TM^A$ site,

and 22 compounds with interactions at the $7TM^B$ site. These were tested for CaSR-induced G_{i3} activation[32] using an extracellular calcium concentration of 0.5 mM. One PAM emerged from those selected for the $7TM^A$ site with > 10% of *Emax* induced by cinacalcet, and three PAMs were found for the $7TM^B$ site, representing hit rates of 3.8% (1/26) and 13.6% (3/22), respectively (**Fig. 1a, 1b**). The higher hit rate for the $7TM^B$ site may be attributed to its more enclosed pocket, which better excluded molecules unlikely to bind and led to better ligand complementarity. While all four compounds physically resemble known PAMs, containing a buried aromatic ring, a bridging cationic linker, and a distal aromatic ring, they were topologically dissimilar to the known ligands in the ChEMBL and IUPHAR databases, with ECFP4 Tc values $\leq$ 0.35 (**Fig. 1c, Extended Data Table 1**). Even though the initial potency of these molecules was low (**Fig. 1d**), we were able to optimize three of them to potencies in the 30-220 nM range (**Fig. 3e**, **Extended Data Fig. 2**), supporting their authenticity as true PAMs.

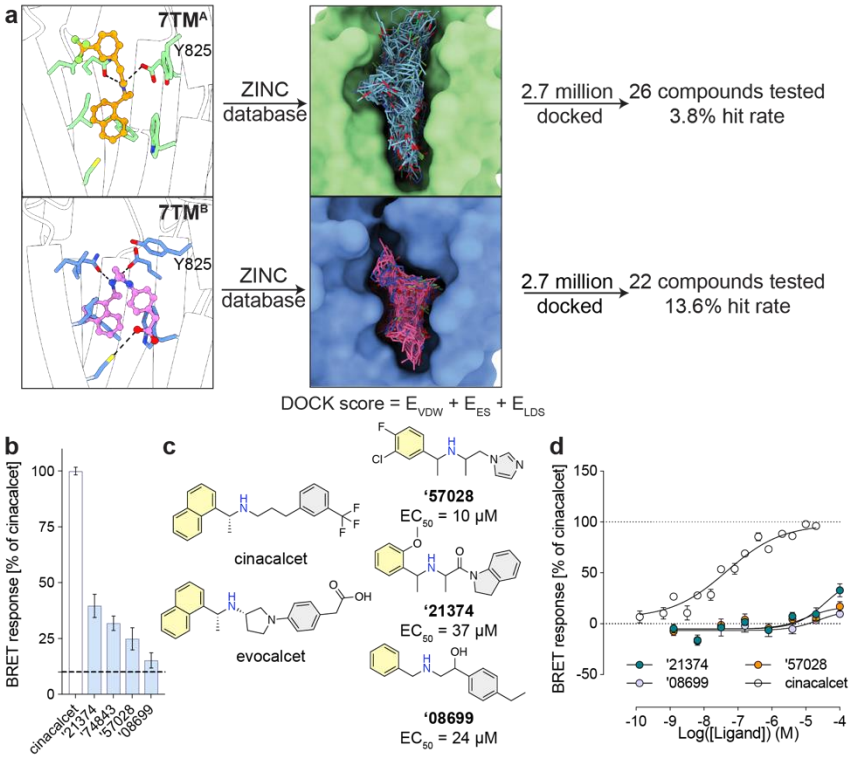

`

Fig. 1: Small-scale in-stock screens in the two 7TM sites of CaSR. a, 2.7 million molecules were docked against the allosteric 7TM sites of CaSR. Docking against $7TM^B$ outperforms $7TM^A$ in terms of higher hit rate (13.6% versus 3.8%). Hit rates were defined by over 10% BRET response compared to cinacalcet at 100 μM. E_{VDW}: van der Waals; E_{ES}: electrostatic; E_{LDS}: ligand desolvation. Cinacalcet is in gold and evocalcet is in pink for illustration of the binding sites (**PDB: 7MCF**). **b,** BRET response (normalized to cinacalcet) of the initial hits at 100 μM. **c,** Examples of the docking hits in comparison to the known PAMs cinacalcet and evocalcet. The new hits have amine (in blue) flanking by hydrophobic groups (yellow: hydrophobic groups that are stationary (either experimentally determined or by docking prediction); grey: hydrophobic groups that can be flexible). **d,** Concentration response curves of the initial hits **'21374**, '**57028** and **'08699**. Estimated EC_{50} for cinacalcet is 46 nM [28 – 74 nM].

Large library docking on CaSR for new chemotypes. To measure the impact of larger libraries, and potentially identify more potent PAMs, we screened a library of 1.2 billion make-on-demand ("tangible") molecules[33] against the more enclosed $7TM^B$ site. Here, an average of 1,706 orientations were sampled for each library molecule, each in an average of 425 conformations, or 682 trillion total configurations overall; this calculation took about 16 days of elapsed time on a 1,000-core cluster. Top-scoring molecules were filtered and clustered as for the smaller library, and 1,002 cluster-heads passed all criteria. 96 molecules that score well in both sites were prioritized for synthesis, of which 74 compounds were successfully made, a 77% fulfillment rate. In BRET assays, 27 of the 74 compounds produced >10% of the *Emax* induced by cinacalcet, a 36.5% hit rate almost three-fold higher than did the 2.7 million molecule library (**Fig. 2a, b**).

The larger library also revealed hit molecules with higher potency than those from the smaller library, with more than 70% having EC_{50} values better than 10 μM, and 20% having an EC_{50} better than 1 μM (**Fig. 2c, Extended Data Table 1**), with the best having an EC_{50} of 270 nM. Given the number of molecules tested, the hit-rate difference between the larger and smaller library screens was significant (p-value < 0.01), and in fact is only as good as it is for the smaller library when we count as hits molecules with EC_{50} values worse than 10 μM. In the 1-10 μM and in the 0.1-1 μM ranges, no hits emerged from the smaller library, whereas multiple ones did so from the larger library. These results support the theoretical studies predicting better performance

`

from larger libraries[34], providing an experimental quantification for the impact of larger versus smaller libraries.

A core goal of this study was finding new chemotypes conferring new pharmacology. We therefore prioritized high-ranking docked molecules based on both potency and topological dissimilarity to known CaSR PAMs (**Fig. 2e-h, Extended Data Table 1**). Thus, while drugs like cinacalcet and evocalcet are characterized by a naphthyl separated from a phenyl by a five-atom cationic linker, the new PAMs explored different and typically heteroaromatic anchors, different linkers, and frequently lacked the methyl α to the cation that is ubiquitous among CaSR PAMs. Naturally, with the spatial and chemical restrictions of these pockets, there were physical resemblances between the established drugs and the new PAMs (**Fig. 2e-h)**. Cryo-EM structures have shown that the cationic amine of cinacalcet and evocalcet hydrogen bonds and ion-pairs with Q681$^{3.33}$ and E837$^{7.32}$ of CaSR, which are critical for PAM recognition[16,35]. Meanwhile, the highly conserved methyl group α to this cationic amine fits into a hydrophobic pocket formed by I841$^{7.36}$, F684$^{3.36}$, F668$^{2.56}$, whose substitutions with alanine abolish or decrease binding affinities for CaSR PAMs[36]. In their bent conformations bound to 7TM^{B}, the naphthalene ring common to both drugs T-stacks with F684$^{3.36}$ and W818$^{6.50}$, while the trifluoromethylbenzene of cinacalcet forms edge-to-pi interaction with W818$^{6.50}$. Remarkably, although their linker lengths differ from the known drugs, most of the new PAMs also adopt “bent” conformations in their docked poses within the 7TM^{B} CaSR pocket (**Fig. 2e-h, Extended Data Fig. 1**). While most of them retain hydrophobic flanking groups that dock into the aryl sites defined by cinacalcet and evocalcet, all do so with different moieties (compare **Fig. 1c** to **Fig. 2e-2h**).

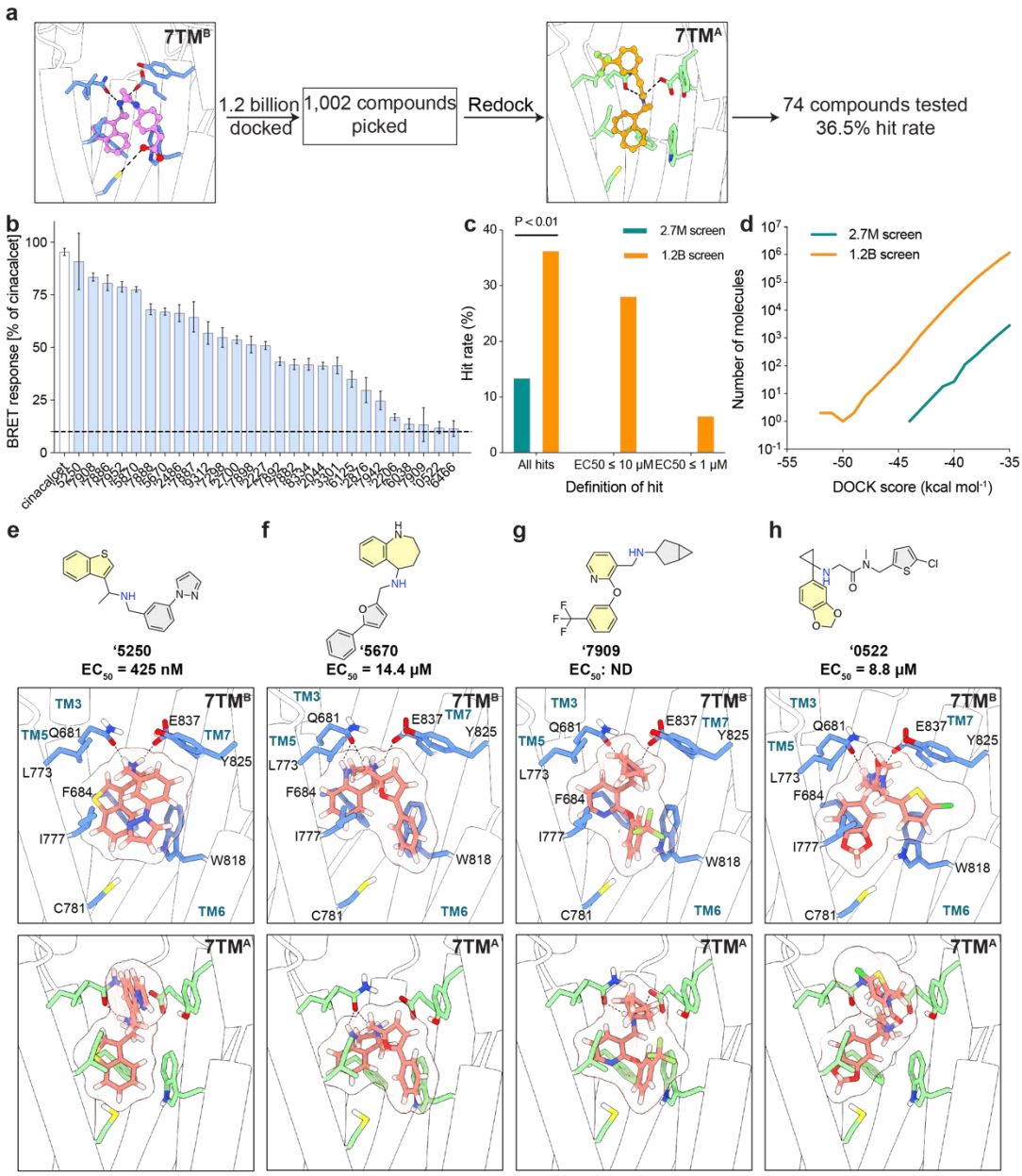

Fig. 2: Novel ligands are identified through docking 1.2 billion make-on-demand library. a, Workflow of an iterative docking campaign against CaSR. All compounds were first docked in the 7TM^B site. **b,** BRET response (normalized to cinacalcet) of the hits. Hit rates were determined by over 10% BRET response (compared to cinacalcet) at 10 μM. **c,** Hit rate comparison between 2.7 million and 1.2 billion screens. The overall hit rate of the 1.2 billion screen is significantly better than the in-stock 2.7 million screen (P < 0.01 by z-test). **d,** Total docking energies of top-scoring molecules out of LSD compared to in-stock screen (only molecules with DOCK score < -35 kcal mol^{-1} are plotted). **e-h,** Representative novel PAMs discovered from docking (colors represent the different moieties that fulfill the same role). **Top:** 2D structures. **Middle:** Docked poses in 7TM^B site. **Bottom:** Docked poses in 7TM^A site.

`

Structure-based optimization of new PAMs. To increase the affinity of the initial hits, we sought to optimize interactions with residues that had proven important in other series[33], including Q681$^{3.33}$, E837$^{7.32}$, I841$^{7.36}$**,** F668$^{2.56}$, F684$^{3.36}$, and W818$^{6.50}$ (**Fig. 3a**). The greater polarity of the docking hits, whose calculated octanol:water partition coefficient (clogP) ranged from 2.3 to 4.0 vs. a clogP of 5.1 for the more hydrophobic cinacalcet, gave us freedom to operate in the hydrophobic CaSR site.

To fill a gap in the interface with L773$^{5.40}$, Y825$^{6.57}$ and to stiffen the linker in the docking-derived PAM **'5250** (EC_{50} 415 nM), a second methyl was added proximal to the cationic nitrogen. This improved potency five-fold, to an EC_{50} of 90 nM, while synthetic resolution of the diastereomers improved it another 130-fold. The resulting compound Z8554052021 (**'2021**), with an EC_{50} of 3.3 nM, is among the most potent CaSR and indeed GPCR PAMs described (**Fig. 3b**).

The tetrahydrobenzapine of compound '**5670** (**Fig. 2f**) separates it from the naphthalene equivalent of cinacalcet and evocalcet and gives it a relatively polar and certainly three-dimensional character compared to the equivalent groups of other CaSR PAMs. Substitution of the terminal phenyl-furan with a more compact and more polar benzothiazole, which can be well-accommodated in the hydrophobic site defined by residues I777$^{5.44}$, W818$^{6.50}$ and Y825$^{6.57}$, improved potency seven-fold (compound Z2592185946 (**'5946**)), while its N-methylation led to **'6218** (EC_{50} 0.25 µM) (**Extended Data Fig. 3b**). Enantiomeric purification led to **'2460**, a 177 nM CaSR PAM (**Fig. 3c**). Despite its 80-fold potency improvement, the molecular weight and cLogP values of **'2460** were actually reduced versus the parental docking hit, improving Lipophilic Ligand Efficiency (LLE) from 0.9 to 3.4. Similar changes in the equivalent aryl groups, binding in the hydrophobic site defined by residues F668$^{2.56}$ and I841$^{7.36}$, led to improvements in docking hits Z5208267909 (**'7909**) and Z1591490522 (**'0522**) (**Fig. 2d, Extended Data Fig. 3c**). For the former, the EC_{50} improved from over 100 µM to 1.7 µM (Z6562953161 (**'3161**)**, Fig. 3d**), and

efficacy was much improved even though molecular weight was, again, decreased. Meanwhile, the analog of **'0522**, Z6923555526 (**'5526**)**,** saw the introduction of the same benzothiazole as in '**2460**, along with a simplification of the linker, giving better complementarity with the hydrophobic site defined by I777$^{5.44}$, W818$^{6.50}$ and Y825$^{6.57}$ **(Extended Data Fig. 3c**), and improving EC_{50} 95-fold, to 0.48 µM.

We also sought to optimize the early PAMs revealed by the "in-stock" library. Although these molecules began with weak EC_{50} values, we were able to optimize three of the four molecules to EC_{50} values 30-163 nM (**Fig. 3e, Extended Data Fig. 2a**). Most compelling was the improvement of **'21374**. Here, simplification of the linker and installation of a benzothiazole, as in **'6218** and **'5526**, above, led to **'85339**, with an EC_{50} of 174 nM**.** Stereochemical purification to (*R)*-**'85339** (**'54149**) revealed a 41 nM PAM. It was this molecule, with relatively high potency (4.5-fold improved on that of cinacalcet), favorable cLogP (2.9), new chemotype, and novel receptor contacts, that we ultimately took forward into *in vivo* studies.

`

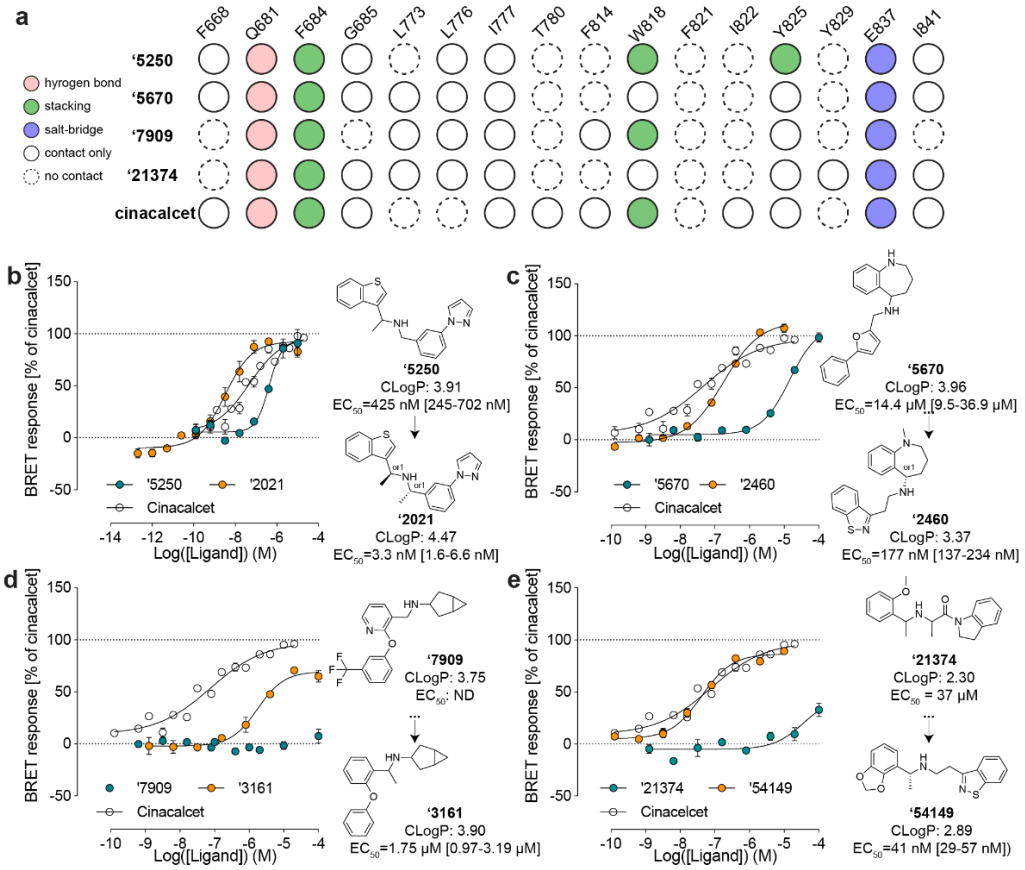

Fig. 3: Initial hits to high-affinity analogs. a, Contact analyses of the initial docking hits versus cinacalcet. **b,** Docking hit **'5250** and its optimized analog **'2021** (a diastereomer of **'6783**). **c,** Docking hit **'5670** and its optimized analog **'2460** (an enantiomer of '6218). **d,** Docking hit **'7909** and its optimized analog **'3161**. **e,** In-stock docking hit **'21374** and its optimized analog **'54149**. EC_{50} was determined by monitoring Gi activation by CaSR upon compound addition at $[Ca^{2+}]$ = 0.5 mM. The efficacy of the compounds is normalized to the maximum BRET response induced by cinacalcet. Data represent means and SEMs of 3-27 replicates.

Cryo-EM structures of the '6218- and '54149-CaSR complexes. To understand the molecular basis of recognition and to template subsequent optimization, we determined structures of CaSR in complex with two PAMs, **'6218** and **'54159** (*R*-**'85339**), derived from the 1.2 billion and the 2.7 million molecule screens, respectively. For CaSR-**'6218** complex, the map was determined at a global nominal resolution of 2.8 Å with locally refined maps at resolutions of 2.7 Å and 3.4 Å for ECD-linker and linker–7TM regions, respectively (**Extended Data Fig. 4 and Fig. 5)**. For CaSR-**'54149** complex, the map was determined at a global nominal resolution of 2.7 Å

`

with locally refined maps at resolutions of 2.6 Å and 3.6 Å for ECD-linker and linker–7TM regions, respectively (**Extended Data Fig. 4** and **Fig. 5**). Similar to the structures of cinacalcet- and evocalcet-bound CaSR complexes[16], the 7TMs between two protomers adopt an asymmetric arrangement characterized by a raised position adopted by the TM6 of $7TM^{A}$ relative to the opposing TM6 of $7TM^{B}$ (**Extended Data Fig. 6A, 6B**).

In the CaSR-**'6218** complex, the PAM binding sites show density of **'6218** in "extended" and "bent" conformations, recapitulating those of cinacalcet and evocalcet (**Fig. 4a, 4c**)[16]. **'6218** interacts with the same overall residues in both monomers, making conserved as well as site-specific interactions. In both sites, the cationic amine of the PAM ion-pairs with $E837^{7.32}$ and hydrogen-bonds with $Q681^{3.33}$. In the $7TM^{B}$ site, the methyl-benzazepine ring forms pi-pi interactions with $F684^{3.36}$ and $W818^{6.50}$, recapitulating the interactions formed by the naphthalene in cinacalcet and evocalcet. The benzoisothiazole ring makes pi-pi interactions with $F821^{6.53}$ and $Y825^{6.57}$ (**Fig. 4c**). In the $7TM^{A}$ site, while $W818^{6.50}$ swings out by 120° and $Y825^{6.57}$ moves down, the pi-pi interactions are still maintained. Conversely, the interaction with $F821^{6.53}$ is lost as it swings out and is no longer part of the allosteric pocket (**Fig. 4a**). The docking predicted pose for **'6218** superposes well with its experimental structure in both monomers (**Fig. 4b, 4d**). Both the docked and experimental poses of **'6218** adopt an "extended" conformation in the $7TM^{A}$ site (**Fig. 4b**), while they have a "bent" conformation in the $7TM^{B}$ site (**Fig. 4d**). The same bent and extended conformations were observed for the initial docking hits; in this sense, this level of geometric fidelity emerged directly from the docking screen (**Fig. 2e-2h, Extended Data Fig. 1**). The docked and experimental structures superimposed with a 1.88 Å root mean square deviation (RMSD) in the bent conformation monomer, and with a 2.23 Å RMSD in the extended conformation monomer. While the experimental results broadly support the docking prediction, there were important differences in the receptor structures. Compared to the cinacalcet complex against which we docked ($7TM^{B}$), $F821^{6.53}$ swings 120° into the site to become part of the binding pocket, making

`

pi-pi interaction with the benzoisothiazole ring of **'6218 (Fig. 4d**). This conformation is not adopted in the cinacalcet or the evocalcet complex, likely because the mobile groups of cinacalcet (1-propyl-3-(trifluoromethyl) benzene) and evocalcet (2-phenylacetic acid) are bulkier and would clash with this phenylalanine (**Extended Data Fig. 7**). Meanwhile, in the "extended" monomer's binding site (7TM^{A}), W818$^{6.50}$ moves 120° to swing outside of the binding pocket in the **'6218** complex.

Similar to **'6218**, **'54149** can adopt an "extended" conformation in the 7TM^{A} site and a "bent" conformation in the 7TM^{B} site, inducing similar rearrangements of W818$^{6.50}$ and F821$^{6.53}$ in the 7TM^{A} and 7TM^{B} site, respectively (**Fig. 4e-4h**). **'54149** and **'6218** share a benzoisothiazole group in their chemical structures that is flexible in the two sites, suggesting the conformational changes of W818$^{6.50}$ and F821$^{6.53}$ are benzoisothiazole specific. At the 7TM^{B} site, the benzodioxole group interacts with F684$^{3.36}$ and W818$^{6.50}$ through pi-pi stacking while the benzoisothiazole forms pi-pi interactions with F821$^{6.53}$ and Y825$^{6.57}$. The cationic amine hydrogen bonds with Q681$^{3.33}$ and ion-pairs with E837$^{7.32}$, and the adjacent methyl packs with I841$^{7.36}$ (**Fig. 4g**). The interactions with F821$^{6.53}$ and Y825$^{6.57}$ are lost in the 7TM^{A} site as F821$^{6.53}$ swings out of the pocket and Y825 swings down (**Fig. 4e**). The docked and experimental structures superposed to 0.91 Å RMSD in the 7TM^{A} site, and to 2.68 Å RMSD in the 7TM^{B} site (**Fig. 4g, h**). Docking predicted **'54149** to adopt both "extended" conformations in the binding pocket but we observe signs of conformational heterogeneity in the 7TM^{A} site. The EM density suggests that **'54149** adopts an alternative "folded-over" conformation at this site, which has never been previously observed (**Extended data Fig. 5c and Extended data Fig. 8**). In this "folded-over" configuration, **'54149** establishes favorable interactions with CaSR—the benzoisothiazole ring makes additional contacts by edge-to-pi stacking with F814$^{6.46}$ and is surrounded by a hydrophobic pocket created by A840$^{7.35}$, I841$^{7.36}$, A844$^{7.39}$ and V817$^{6.49}$. Among those residues, A840$^{7.35}$ and I841$^{7.36}$ are important for the affinity of CaSR PAMs[35,36]. Unlike methyl-benzazepine (in **'6218**) and naphthalene (in cinacalcet and evocalcet), **'54149** uses a smaller benzodioxole as the stationary

`

binding component, possibly allowing more configurations in the pocket. Together, the conformational disparity in the structure of these complexes highlights the ongoing importance of cycles of docking and structure determination in drug discovery efforts.

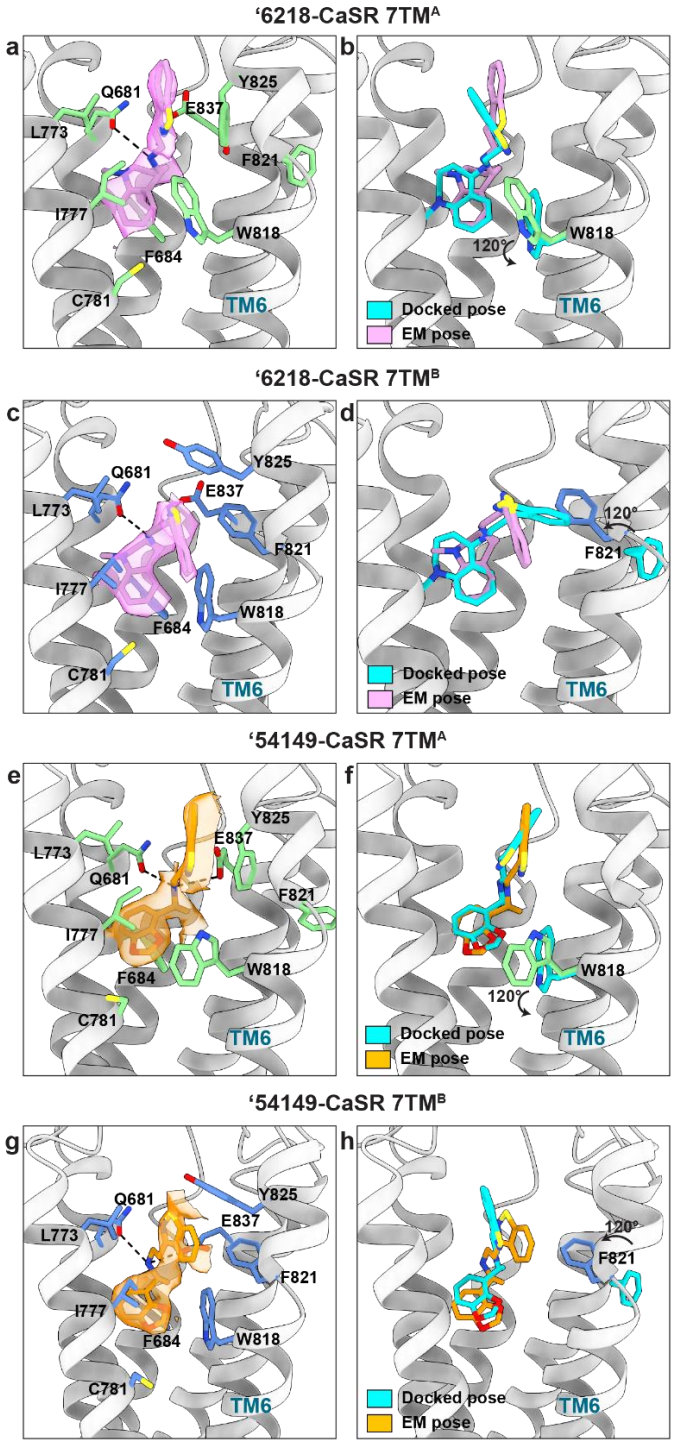

`

Fig. 4: Structural comparison between docked and experimentally determined poses for '54149 and '6218. a, Close-up view of **'6218** in the 7TM^{A} site, with its EM density shown. Surrounding residues are in green. **b,** Superposition of docked and experimentally determined pose of **'6218** in the 7TM^{A} site. **c,** Close-up view of **'6218** in the 7TM^{B} site, with its EM density. Surrounding residues are shown in blue. The docked pose and its surrounding residues are in silver. **d,** Superposition of docked and experimentally determined pose of **'6218** in the 7TM^{B} site. **e,** Close-up view of **'54149** in the 7TM^{A} site, with its EM density. The surrounding residues are in green. **f,** Superposition of docked and experimentally determined pose of **'54149** in the 7TM^{A} site. **g,** Close-up view of **'54149** in the 7TM^{B} site, with its EM density. The surrounding residues are in blue. **h,** Superposition of docked and experimentally determined pose of **'54149** in the 7TM^{B} site. (**b**, **d**, **f**, **h**) The residues undergoing conformational changes in the experimental structures are shown. Docked poses and protein residues in the docked structures are in cyan.

'54149 stabilizes a distinct active-state CaSR dimer conformation. Compared to CaSR-cinacalcet alone, the structure against which we docked, our recent structure of the receptor in complex with cinacalcet and Gi$\beta\gamma$ (He et al., *accepted manuscript*, PDB: 8SZH) revealed that G protein binding promotes an additional conformational change that brings the two 7TMs into closer contact, in a configuration that is in line with the activation of other Family C receptors[17,37]. From the inactive state to the G-protein-bound active state, the interface contact area increases from 178.9 Å^2 (inactive; NPS-2143 bound; PDB: 7M3E) to 206.2 Å^2 (cinacalcet-bound; PDB: 7M3F) to 682.7 Å^2 (cinacalcet, Gi$\beta\gamma$-bound) (calculated by PDBePISA). By aligning the 7TM^{B}s, **'54149** and **'6218**'s 7TM^{A} moves down towards the cytoplasm associated with an increase in interface contact area to 351.3 and 271.5 Å compared to cinacalcet-bound CaSR, as illustrated by the relative positioning of the TM6 helices (**Fig. 5a**). The downward shift brings the two 7TMs in a conformation that is closer to the G protein-bound structure, especially for that induced by **'54149**, suggesting that **'54149** promotes a dimer configuration that may favor G-protein activation compared to those stabilized by the other compounds **(Extended data Fig. 9)**. This may contribute to its efficacy and also potentially confer a different pharmacology.

'54149 suppresses PTH secretion better than the approved PAM drugs. Upon its activation, CaSR suppresses PTH secretion from parathyroid glands[38], which is the primary target of calcimimetic drugs. Since all PAM-bound structures were obtained under saturating calcium concentrations (10 mM), the different conformations observed are specific to each PAM and may be reflected in measurable functional differences. We thus investigated the functional effects of the different PAM drugs and leads by monitoring PTH secretion in extracted parathyroid glands

`

from wild-type (WT) C57/BL6 (B6) mice at a constant external calcium concentration of 0.75 mM. All three of '**54149**, cinacalcet, and evocalcet inhibit PTH secretion dose-dependently, with potencies of **'54149** (583 nM) ~ evocalcet (998 nM) >> cinacalcet (53 μM) (**Fig. 5b**). As PAMs positively regulate CaSR by lowering the required calcium for activation, we wanted to assess how the different compounds shift the calcium set point for PTH secretion by the glands (**Fig. 5c, 5d**). For this assay we used two PAM concentrations, 500 and 50 nM, (dashed line in **Fig. 5b**). At 500 nM, **'54149** shifted the calcium set point from 1.5 mM to 0.62 mM, while at the same concentration, cinacalcet shifted the set point to ~0.94 mM and evocalcet shifted it to 0.76 mM (**Fig. 5d**). The same trend holds when the PAMs were administered at 50 nM, leading to shifts in the calcium set-point from 1.47 (vehicle) to 1.23 (cinacalcet) to 1 (evocalcet) to 0.85 (**'54149**) mM (**Fig. 5c**). It is worth noting that **'54149** also suppresses the tonic secretion of PTH at 0.5 mM calcium, an effect not observed with the two approved drugs.

`

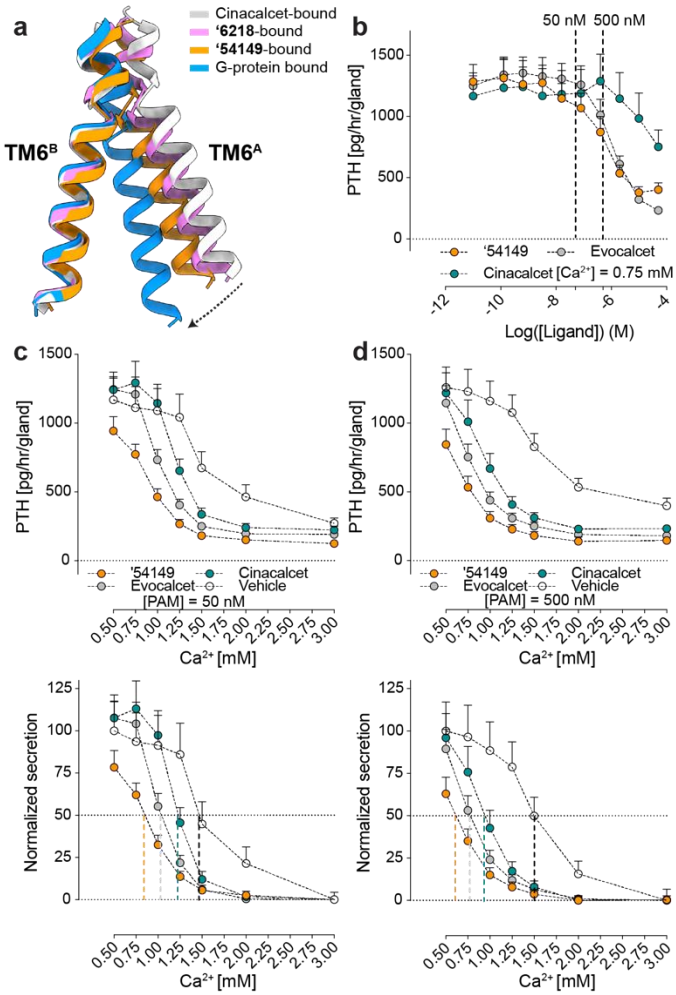

368

369 **Fig. 5: '54149 increases the TM6-TM6 interface and is more effective in suppressing**
370 **PTH secretion in *ex vivo* parathyroid glands. a,** The $7TM^A$ protomer experiences a downward
371 and rotational movement bringing TM6 closer to the $7TM^B$ from cinacalcet-bound to **'54149**-bound
372 structure to Gi-bound CaSR. Cinacalcet-bound CaSR is in grey, **'54149**-bound CaSR is in orange,
373 **'6218**-bound CaSR is in pink and Gi-bound CaSR is in blue. **b,** Parathyroid glands of 4-week-old
374 C57/B6 wild-type (B6:Wt) mice were sequentially incubated with increasing concentrations of
375 **'54149**, cinacalcet and evocalcet from 0.01 nM to 50 μM in the presence of 0.75 mM $[Ca^{2+}]_e$. The
376 IC_{50}s of **'54149**, evocalcet and cinacalcet in suppressing PTH secretion are 583 nM [122 -4727
377 nM], 998 nM [412 – 4018 nM] and 53 μM respectively. **c, d,** Parathyroid glands were sequentially
378 incubated with increasing $[Ca^{2+}]_e$ from 0.5 mM to 3.0 mM in the presence of vehicle (0.1% DMSO),
379 50 nM (**c**) or 500 nM (**d**) of **'54149**, cinacalcet or evocalcet. Top panels show changes in the rate
380 of PTH secretion on a per-gland and per-hour basis with raising $[Ca^{2+}]_e$ to compare the PTH-max.
381 Bottom panels show normalized PTH secretion rate (the highest rates are normalized to the basal
382 rate at 0.5 mM $[Ca^{2+}]_e$ of the vehicle and the lowest rates are normalized to the rate at 3.0 mM
383 $[Ca^{2+}]_e$) to better assess changes in the Ca^{2+}-set-point ($[Ca^{2+}]_e$ needed to suppress 50% of $[Ca^{2+}]_e$-
384 suppressible PTH secretion). Dotted vertical lines indicate Ca^{2+}-set-points for the corresponding
385 treatments. Mean $\pm$ SEM of n = 8 groups of PTGs for each treatment.
386

`

‘54149 reduces serum PTH at lower doses with less hypocalcemia than cinacalcet

Encouraged by its improved affinity and *ex vivo* organ efficacy, we investigated the *in vivo* activity of ‘**54149**, beginning with pharmacokinetic (PK) studies in CD-1 mice. We administered ‘**54149** at a dose of 3 mg/kg subcutaneously, and dosed cinacalcet and evocalcet in the same manner for direct comparison (**Fig. 6a**). At this dose, ‘**54149** was found in appreciable amount in plasma—$AUC_{0\rightarrow inf}$ 18,500 mg*min/ml. The C_{max} reaches 112 ng/ml (**340 nM**) at 15 min and stays high until 60 min (100 ng/ml). Based on ‘**54149**’s EC_{50}, ‘**54149** is close to saturation at 3 mg/kg dose over this period (**Fig. 3f**). By comparison, evocalcet has a much higher systemic exposure at the same dose, with a C_{max} of 3,250 ng/ml (**8.68 µM**) at 60 min. On the other hand, cinacalcet - which is far more widely used - has lower exposure than ‘**54149**, with C_{max} of 58.9 ng/ml (**149.5 nM**) 15 min after subcutaneous administration (**Fig. 6a**). We note that no effort has been made to optimize ‘**54149** for pharmacokinetic exposure or clearance—to the extent that it has favorable PK, this simply reflects the physical property constraints imposed in docking and ligand optimization.

Based on the PK, we picked two doses to investigate the time course of PTH suppression by the PAMs in WT B6 mice. At 1 mg (3.1 µmol/kg), ‘**54149** and equimolar evocalcet fully suppress PTH secretion, while cinacalcet is less effective at this dose (**Fig. 6b**). Only at 10 mg/kg (31 µmole/kg) was cinacalcet able to fully suppress PTH secretion (**Fig. 6c, 6d**). Overall, **‘54149** fully suppresses serum PTH at 10 times lower dose than cinacalcet (**Fig. 6d**), consistent with its ability to suppress releases of both tonic and Ca^{2+}-suppressible pools of PTH (**Fig. 5c, 5d**).

A key adverse effect of cinacalcet and etelcalcetide is decreased blood calcium[39]. In secondary hyperparathyroidism (SHPT), high PTH is accompanied by low or normal blood calcium concentration. The overproduction of PTH and the proliferation of parathyroid cells in patients with SHPT are largely driven by low blood calcium and high blood phosphate levels[40-42]

`

as well as reduced CaSR expression in parathyroid cells[43]. We were thus keen to compare the serum calcium concentration after injection of '**54149** versus cinacalcet. At the dose of 3mg/kg, '**54149** did not significantly alter serum calcium concentration for 4 hrs, but slightly increased it from 2.2 to 2.4 mM after the drug dissipated in circulation 6 hrs post-injection (**Fig. 6e**). In contrast, the same dose of cinacalcet and evocalcet significantly lowered serum calcium for more than 8 hrs from 2.2 mM to the lowest levels of 1.7 mM and 1.6 mM, respectively. The hypocalcemic action of evocalcet is particularly robust even at a lower dose of 3.1 µmol/kg (~1 mg/kg) (**Fig. 6f**), while the same dose of **'54149** retained the ability to maximally suppress serum PTH without producing hypocalcemia (**Fig. 6d**). Although the mechanisms underlying the different calcemic actions of these 3 compounds remain to be determined, their common ability to suppress PTH secretion suggests that differential calcemic actions likely take place in other calciotropic organs outside of parathyroid glands.

`

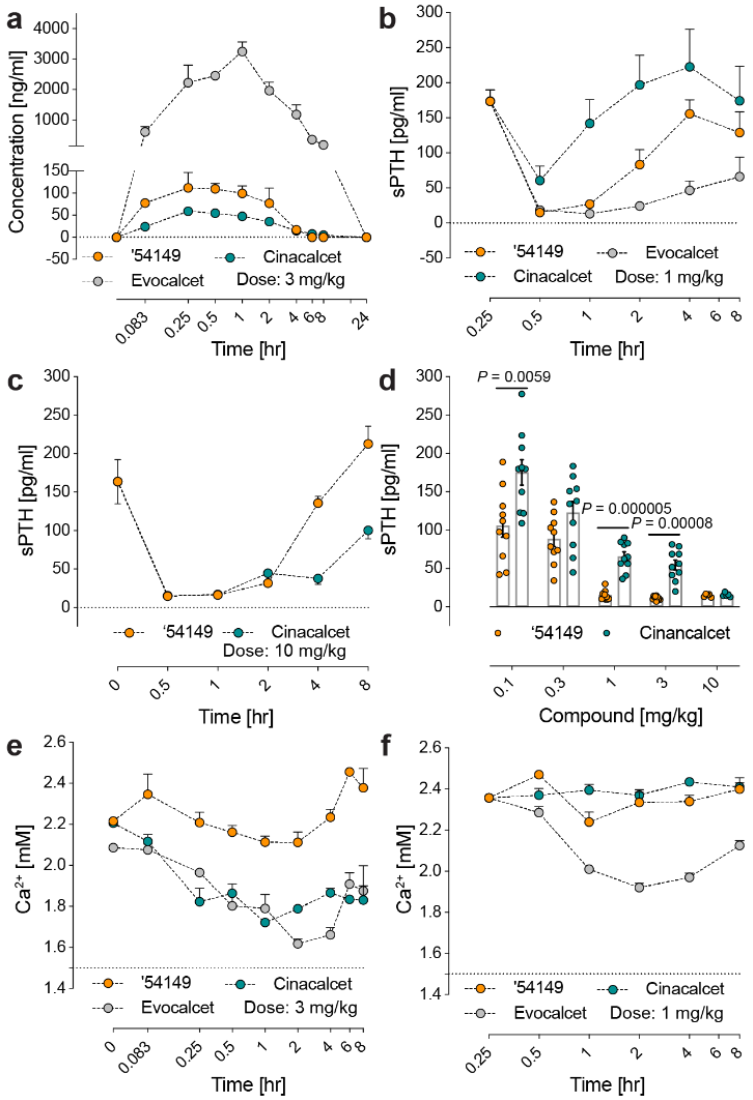

Fig. 6: '54149 suppresses serum PTH at lower dose and causes less hypocalcemia effect than cinacalcet and evocalcet. a, Pharmacokinetics of **'54149** compared to cinacalcet and evocalcet after 3 mg/kg subcutaneous injection. **b,** Serum PTH concentration change over 8 hours after 1 mg/kg subcutaneous injection of **'54149**, cinacalcet or evocalcet. **c,** Serum PTH concentration change over 8 hours after 10 mg/kg subcutaneous injection **'54149** or cinacalcet (n = 5). **d,** Comparison of **'54149** to cinacalcet in regulating serum PTH at different doses (subcutaneous injection) after 30min of injection. Each dose consists of n = 10 mice except injection at 10 mg/kg (n = 5). P-values were assessed by unpaired Student's t-test. **e,** Plasma calcium concentration in mice after 3 mg/kg subcutaneous injection of **'54149**, cinacalcet or evocalcet. **f,** Serum calcium concentration after 1 mg/kg subcutaneous injection of **'54149**, cinacalcet or evocalcet. For experiments in panel **b-d**, **f**, the concentrations of evocalcet and cinacalcet are corrected for their molecular weight difference with **'54149**.

`

Discussion

Four key observations emerge from this study. **First**, from a structure-based screen of a 1.2 billion molecule tangible library emerged a spectrum of diverse chemotypes that potently enhanced CaSR activation. The new molecules represent among the first positive allosteric modulators (PAMs) discovered via large library docking, and among the first structure-based ligands discovered for Family C GPCRs. The potency of the initial docking hits was relatively high, with EC_{50} values down to 270 nM, and all were topologically dissimilar to known CaSR PAMs. Structure-based optimization improved affinity between 40 and 600-fold, leading to molecules that were up to 50-fold more potent than cinacalcet *in vitro* and 10 to 100-fold more potent at suppressing PTH secretion from organs *ex vivo* as well as *in vivo* in animals. **Second**, the docking predictions were largely confirmed by the subsequent cryo-EM structures, with an important exception (see below), including selecting for and correctly predicting extended and bent conformations in the TM^A and TM^B sites of the CaSR dimer. **Third,** our direct comparison for the impact of docking an ultra-large (1.2 billion) library versus a smaller (2.7 million) molecule library in the same pocket shows the improvement in docking scores as the library size increases, an effect that has been previously suggested by simulations[34] but not experimentally tested in a controlled way (**Fig. 2d**), Here, experimental docking hit rates were 2.7-fold higher in the large library screen than in the "in-stock" screen, and the best hits from the large library were up to 37-fold more potent. **Fourth,** the new chemotypes make new interactions with the receptor, promoting new active-state dimer interfaces that are closer to the G-protein coupled state which were not observed with the established drugs. In this sense, the experimental structures provide an additional layer of information in terms of global conformations that may help explain differences in the relative efficacy and pharmacology of different ligands. Correspondingly, **'54149** promotes a TM6-TM6 interface that is closest to the fully active G-protein coupled state of the receptor dimer and is highly potent in suppressing PTH secretion, while also seemingly devoid of the hypocalcemia that is the key dose-limiting side effect of approved calcimimetic drugs[44,45].

`

Several caveats merit mentioning. We do not pretend the molecules described here are drugs, or even drug candidates. Whereas the pharmacokinetics of **'54149** are sufficient to support *in vivo* studies, and indeed in some ways to demonstrate superiority to cinacalcet, there is clearly room for optimization of exposure and half-life of the molecule. While the relative lack of a hypocalcemic effect is very encouraging, understanding the mechanism underlying this effect requires systematic exploration of CaSR activation in other calciotropic organs, including bones and kidneys. Further, whereas in three of the four cases the docking predicted structures of the PAMs in the $7TM^A$ and $7TM^B$ monomers were confirmed by cryo-EM, in one site the docking pose was different from the experimental result. Finally, while the improvement in docking hit rates and docking potencies from billion molecules versus million molecule libraries seems compelling, the numbers experimentally tested remain relatively low given the docking uncertainties. A more expanded and strongly powered assessment merits investigation.

These caveats should not obscure the main observations: From docking 1.2 billion molecules against the structure of CaSR emerged potent new positive allosteric modulators, topologically dissimilar to the known ligands of this receptor. Structure-based optimization of the new PAMs led to molecules with *in vitro* potencies in the low nM range, up to 14-fold more potent than the standard of care for the calcimimetic drugs, cinacalcet. In *ex-vivo* organ studies this increase in potency was retained, while *in vivo*, too, the new molecules were also substantially more potent than cinacalcet. The novel chemotypes stabilized CaSR dimer conformations that are not observed in the previous structures of established PAMs, which may underlie the ability of the new chemotypes to support strong efficacy in suppressing parathyroid hormone secretion without inducing their dose-limiting hypocalcemia. Finally, docking hits were 37-fold more potent, and docking hit-rates 2.7-fold higher in the billion-molecule library campaign than for docking the million-molecule scale library against the same site. While such a comparison merits further study,

`

certainly with more molecules being tested, it is consistent with theoretical studies[34], and supports the continued expansion of readily testable libraries for drug discovery[20,23].

Acknowledgements

This work is supported by US NIH grants R01 NS122394, and R01 DK132902 (to G.S), R35GM122481 (to BKS), R01GM133836 (to JJI), RF1AG075742, R01DK122259, BLR&D I01BX005851 and IK6BX004835 (to WC), Damon Runyon Postdoctoral Research Fellowship (to FL).

Author Contributions

F.L. conducted the docking screens and the ligand optimization, advised by B.K.S. C.G.W. conducted the *in vitro* activity assays, with early assistance from J.M., and determined the structures by cryo-EM, advised by G.S. C.-L.T., Z.C., and W.C. conducted *ex vivo* and *in vivo* activity assays. Aggregation studies were conducted by I.G. A.L.K. and J.L. assisted the docking screens. J.J.I. developed and prepared the make-on-demand library assisted with large library docking strategies.

Competing Interests

B.K.S. is a founder of Epiodyne Inc, BlueDolphin LLC, and Deep Apple Therapeutics, serves on the SAB of Schrodinger LLC and of Vilya Therapeutics, on the SRB of Genentech, and consults for Levator Therapeutics, Hyku Therapeutics, and Great Point Ventures. G.S. is a founder and consultant of Deep Apple Therapeutics.

`

Data, Code & Material Availability

DOCK3.7 and DOCK3.8 are available without charge for academic use https://dock.compbio.ucsf.edu/. Most underlying data from this study are included among the primary figures and tables, and in the SI, any not so included are available from the authors on request. All molecules tested are available from Enamine and may be accessed via their ZINC numbers (SI Tables 1). Plasmids and reagents to conduct BRET signaling assays are available from G.S. Mouse lines are available from Jackson Laboratory.

Materials and Methods

In-stock and ultra-large virtual ligand screening

To investigate the effect of small versus large library docking and test the docking prediction of the positive allosteric modulator (PAM) binding sites in complex with “extended” or “bent” PAMs, we optimized two docking set ups based on the cryo-EM structures of cinacalcet- or evocalcet-bound CaSR. CaSR/cinacalcet (PDB: 7M3F) is used for $7TM^A$ site, and CaSR/evocalcet (PDB: 7M3G) is used for $7TM^B$ site[16]. In both sites, the position of Q681 and E837 are manually adjusted to form stronger hydrogen bonds or salt bridge with the secondary amine in cinacalcet or evocalcet, and in the $7TM^B$ site, lipid tails were added in the docking set up based on the existing electron density. 7TMs were protonated using Reduce[46] ($7TM^B$ site) or by Protein Preparation Wizard in Maestro ($7TM^A$ site) (2020 release)[47]. Energy grids for the different energy terms of the scoring function were pre-generated--van der Waals term based on the AMBER force fields using CHEMGRID[27]; Poisson–Boltzmann-based electrostatic potentials using QNIFFT73[29,48]; context-dependent ligand desolvation was calculated using SOLVMAP[30]. The volume of the low dielectric and the desolvation volume was extended out 0.8 and 0.3 Å in $7TM^A$ site and 0.6 and 0.3 Å in $7TM^B$ site. The experimentally determined poses of cinacalcet and evocalcet were used to

generate matching spheres, which are later used by the docking software to fit pre-generated ligands' conformations into the small molecule binding sites[26].

The resulting docking set-ups were evaluated for its ability to enrich known CaSR ligands over property-matched decoys. Decoys are theoretical non-binders to the receptor as they are topologically dissimilar to known ligands but retain similar physical properties. We extracted 10 known PAMs from CHEMBL (https://www.ebi.ac.uk/chembl/) including cinacalcet and evocalcet. Four-hundred and eighty-five decoys were generated by using the DUDE-Z pipeline[49]. high logAUCs of 38.89 and 31.67 were achieved for $7TM^A$ site and $7TM^B$ site respectively. Moreover, these docking set-ups offer fidelity in reproducing "extended" and "bent" poses of the known PAMs. For example, by using the $7TM^A$ site set-up, 7 out of 10 PAMs adopt an "extended" conformations, while making sensible interactions with the surrounding key residues. By using the $7TM^A$ site set-up, 7 out of 10 PAMs adopt an "bent" conformations. We also used "extrema" set of 92,552 molecules using the DUDE-Z web server (http://tldr.docking.org) to ensure that the set ups do not enrich extreme physical properties. Both set ups enrich over 90% neutrals or mono-cations among the top-ranking molecules, which are two charges that have precedents of acting as CaSR PAMs.

2.7 million "lead-like" molecules (molecular weight 300-350 Da and logP $\leq$ 3.5), from ZINC15 database (http://zinc15.docking.org/), were docked against both sites using DOCK3.7[26]. In the docking screen against the $7TM^A$ site, each library molecule was sampled in about 3,927 orientations and, on average, 330 conformations. For the $7TM^B$ site, each library molecule was sampled in about 3,612 orientations and, on average, 330 conformations. The best scoring configuration for each docked molecule was relaxed by rigid-body minimization. The two screens took 956 and 917 core hours respectively spread over 100 cores, or slightly more than 3 days. For the 1.2-billion ultra-large library docking, each library from the ZINC22 database[33] was sampled in about 1,707 orientations and 425 conformations in the $7TM^B$ site by using DOCK3.8[26].

`

Overall, over 681 trillion complexes were sampled and scored, spending 380,016 core hours spreading over 2,000 cores, or around 7 days.

Docking results' processing

For the in-stock screen against the $7TM^B$ site, 5,208 molecules with dock energy ≤ -35 kcal/mol were filtered for novelty using the ECP4-based Tanimoto coefficient (Tc) against 662 CaSR ligands in CHEMBL (https://www.ebi.ac.uk/chembl/). Molecules with Tc > 0.35 were eliminated. These molecules are filtered for internal strains with criteria of total strain energy < 8 and maximum dihedral torsion energy < 3[31]. Moreover, the molecules are further filtered for key interactions: hydrogen bond with Q681, salt bridge with E837 by interfilter.py based on OpenEye Python Toolkits (https://docs.eyesopen.com/toolkits/python/quickstart-python/linuxosx.html). After these three filters, 103 molecules were left for further examination. Upon clustering by an ECP4-based *Tc* of 0.5, 79 molecules were visually inspected for pi-pi interactions with W818 and F684. 28 molecules were picked, but only 22 molecules can be sourced from vendors and arrived for *in vitro* testing.

For the in-stock screen against the $7TM^A$ site, 33,321 molecules with dock energy ≤ -43 kcal/mol were filtered against the same three filters, resulting in 2,540 molecules for further examination. The 2,540 molecules were filtered against a vendor filter to assess their persuasibility, resulting in 647 molecules for further examination. The 647 molecules were clustered based on ECP4-based *Tc* of 0.5 and result in 413 clusterheads. The clusterheads were visually inspected in a similar manner resulting in 28 candidates ordering for purchasing, and 26 molecules arrived for testing. For the large-scale screen, 1.2 billion molecules were screened, and 1 billion molecules scored in the $7TM^B$ site. The strain filter is incorporated as part of the new DOCK3.8 pipeline. 2,321,171 molecules with ≤ -35 kcal/mol were filtered for key interactions with Q681, E837, W818 and F684 and novelty. The interaction filtering script for pi-pi interactions with W818 and F684 is

`

implemented based on LUNA (https://github.com/keiserlab/LUNA)[50]. After visual inspection, 1,002 molecules were left. To reduce the number of candidate molecules for purchasing, these 1,002 molecules were re-docked against the $7TM^A$ site, and 907 molecules were scored in the $7TM^A$ site. To the end, the molecules were visually inspected again for their poses against both sites, and the remaining 212 novel and non-strained molecules were clustered by the LUNA 1,024-length binary fingerprint of a *Tc* = 0.3, resulting in 112 clusterheads. Ultimately, 96 molecules were prioritized for purchasing based on a final round of visual inspection. The 96 molecules belong to three categories—(1) molecules that have 2 aromatic ends, and they usually adopt "bent" pose in $7TM^B$ site and "extended" pose in $7TM^A$ site. (2) molecules that have aromatic moiety in the pocket and non-ring structure at the distal end but scores well. (3) interesting or neutral molecules.

Synthesis of molecules

The in-stock prioritized molecules were sourced from Enamine, Vitas-M laboratory, Ltd., UkrOrgSynthesis Ltd., ChemBridge Corporation and Sigma. Ninety-six molecules prioritized for purchasing were synthesized by Enamine for a total fulfilment rate of 74%. Compounds were sourced from the Enamine REAL database (https://enamine.net/compound-collections/real-compounds). The purities of active molecules were at least 90% and typically above 95%. The detailed chemical synthesis can be found in the Chemical Synthesis and analytical investigations section.

Hit Optimization

Potential analogs of the hits were identified through a combination of similarity and substructure searches of the SmallWorld (https://sw.docking.org/) from the 46 billion make-on-demand library. Potential analogs were docked to the CaSR $7TM^B$ binding site using DOCK3.8. As was true in the

`

primary screen, the resulting docked poses were manually evaluated for specific interactions and compatibility with the site, and prioritized analogs were acquired and tested experimentally.

Pharmacokinetics

Pharmacokinetic experiments of **'54149**, cinacalcet and evocalcet were performed by Bienta Enamine Biology Sciences (Kiev, Ukarine) in accordance with the Study Protocols P092622a, P050723b and P050723a. Plasma pharmacokinetics of **'54149**, cinacalcet and evocalcet were measured after a single 3 mg/kg dose, administered subcutaneously (SC) at time points of 5, 15, 30, 60, 120, 240, 360, 480 and 1,440 min. All animals were fasted for 4h before dosing. **'54149** was formulated in 2-HPbCD – saline (30%:70%, v/v). Cinacalcet and evocalcet were formulated in DMSO – 20% Captisol in saline w/v (10:90, v/v). Testing was done in healthy male CD-1 mice (9 weeks old) weighing 32.7 ± 2.1 g, 32.8 ± 1.9 g or 32.9 ± 2.4 g in the three studies. For all three studies, each of the time point treatment group included 3 animals with a control group of one animal dosed with vehicle. In total, 28 animals were used in each study. Mice were injected IP with 2,2,2-tribromoethanol at the dose of 150 mg/kg prior to drawing the blood. Blood collection was performed from the orbital sinus in microtainers containing K3EDTA and tubes with clot activator. Animals were sacrificed by cervical dislocation after the blood samples collection. Blood samples were centrifuged for 10 min to obtain plasma (15 min to obtain serum) at 3000 rpm. All samples were immediately processed, flash-frozen and stored at -70°C until subsequent analysis. The concentrations of the test compound below the lower limits of quantitation (LLOQ = 2 ng/ml) were designated as zero. The pharmacokinetic data analysis was performed using noncompartmental, bolus injection or extravascular input analysis models in WinNonlin 5.2 (PharSight). Data below LLOQ were presented as missing to improve validity of T1/2 calculations. For each treatment condition, the final concentration values obtained at each time point were analyzed for outliers using Grubbs' test with the level of significance set at $p < 0.05$.

`

Sample Processing: Plasma samples (40 µl) were mixed with 200 µl of internal standard solution. After mixing by pipetting and centrifuging for 4 min at 6,000 rpm, 2 µl of each supernatant was injected into LC-MS/MS system. Solution of compound Verapamil (200 ng/ml in water-methanol mixture 1:9, v/v) was used as internal standard for quantification of **'54149** in plasma samples. Solution of Prometryn (100 ng/ml in water-methanol mixture 1:9, v/v) was used as internal standard for quantification of cinacalcet in plasma samples. Solution of Imipramine (50 ng/ml in water-methanol mixture 1:9, v/v) was used as internal standard for quantification of evocalcet in plasma samples.

Data Analysis: Peak plasma concentration (C_{max}) and time for the peak plasma concentration (T_{max}) were the observed values. The areas under the concentration time curve (AUC_{last} and AUC_{inf}) were calculated by the linear trapezoidal rule. The terminal elimination rate constant, ke was determined by regression analysis of the linear terminal portion of the log plasma concentration-time curve. Mean, SD and %CV was calculated for each analyte.

Serum Calcium Measurement: Serum Calcium level was determined using commercial kits according to the manufacturer's instructions. The principle of the method is the ability of calcium forms a blue-colored complex with Arsenazo III dye at neutral pH, the intensity of which is proportional to the concentration of calcium. Interference with magnesium is eliminated by the addition of 8-hydroxyquinoline-5-sulfonic acid. Reproducibility: CV=2.91 %.

Molecular cloning

Full-length (FL) and the truncated CaSR (residues 20-894), were cloned into a pFastBac1 vector (for expression in insect cells) or a pcDNA3.1(+) vector (for expression in HEK293S cells), with a N-terminal haemagglutinin (HA) signal sequence followed by a FLAG tag. To improve the protein yield of CaSR, the DNA sequence of the C-terminal tail from $GABA_{B1}$ or $GABA_{B2}$ and an

`

endoplasmic reticulum retention motif were inserted at the C-terminus of pFastBac1-FLAG-CaSR (20-894) to generate CaSR-C1 and CaSR-C2 constructs, which have been shown to have comparable G-protein signaling profiles as the WT CaSR homodimer[16]. The FLAG tag of CaSR-C1 construct was then replaced by a Twin-Strep-tag (WSHPQFEKGGGSGGGSGGSAWSHPQFEK). All plasmids used were sequence-verified.

Bioluminescence Resonance Energy Transfer (BRET) TRUPATH Assay

BRET assays were performed and analyzed similar to previously described methods[32]. HEK-293S cells grown in FreeStyle 293 suspension media (ThermoFisher) were co-transfected with 150 ng of pCDNA3.1-CaSR FL, Gαi3, Gβ-Rluc8, and Gγ-GFP2 per 1ml of cells at a density of 1 x 10^6 cells ml^{-1} using a DNA/polyethylineimine ratio of 1:5, and incubated at 130 rpm., 37 °C. Cells were harvested 48 h post-transfection, washed in assay buffer (Hank's balanced salt solution with 25 mM HEPES pH 7.5) supplemented with 0.5 mM EGTA, followed by another wash in assay buffer. The cells were then resuspended in an assay buffer with 5 µg ml^{-1} coelenterazine 400a (GoldBio) and placed in white 96-well plates (136101, Thermo Scientific) in a volume of 60 µl per well. 30 µl of ligands prepared at 3-times the final concentrations in assay buffer with 1.5 mM $CaCl_2$, 0.1% BSA, and 3% DMSO were added to plated cells (final concentrations of 0.5 mM $CaCl_2$, 0.33% BSA, and 1% DMSO). After 5 minutes of incubation, the emission at 410 and 515 nm were read using a SpectraMax iD5 plate reader with a 1-s integration time per well. The BRET ratios (GFP2/RLuc8 emission) were calculated and normalized to ligand-free control before further analysis. The efficacy and potency of the molecules were calculated by fitting the concentrations of molecules and the BRET ratios to a four-parameter logistic equation in Prism (Graphpad Software).

`

Protein expression and purification

CaSR-C1 and CaSR-C2 were overexpressed in *Spodoptera frugiperda* Sf9 cells using a Bac-to-Bac baculovirus expression system. Sf9 cells grown to a density of 3 x 10^6 cells ml^{-1} were co-infected with CaSR-C1 and CaSR-C2 baculoviruses for 48 h at 27°C. Cells were then harvested and stored at −80° C. Purifications of CaSR in complex with compounds '54159 and '6218 followed a similar protocol. Cell pellets were thawed, resuspended, and lysed by nitrogen cavitation in the lysis buffer containing 20 mM HEPES pH 7.5, 150 mM NaCl, 10 mM $CaCl_2$, 10% glycerol, 10 mM L-Trp, protease inhibitors, benzonase, and 50 μM of a specific compound. The lysates were centrifuged at 1,000g for 10 min to remove nuclei and unlysed cells. The membranes were harvested by centrifugation at 100,000g for 30 min and solubilized in the lysis buffer supplemented with 1% (w/v) Lauryl Maltose Neopentyl Glycol (LMNG, Anatrace) and 0.2% (w/v) cholesteryl hemisuccinate (CHS, Anatrace) for 3 h, followed by the centrifugation at 100,000g for 30 min. The supernatant was incubated with Strep-Tactin®XT 4Flow® resin (IBA) for overnight at 4°C. The resin was then loaded into a gravity column and washed with 10 column volumes of the washing buffer containing 20 mM HEPES 7.5, 150 mM NaCl, 10 mM $CaCl_2$, 5% glycerol, 40 μM L-Trp, and 50 μM compound, supplemented with 0.01% (w/v) LMNG and 0.002% (w/v) CHS, followed by a second wash with 10 column volumes of washing buffer with 0.001% (w/v) LMNG and 0.0002% (w/v) CHS. Proteins were eluted by Strep-Tactin®XT elution buffer (IBA) supplemented with 10 mM $CaCl_2$, 40 μM L-Trp, 50 μM compound, 0.00075% (w/v) LMNG, 0.00025% (w/v) GDN (CHS, Anatrace) and 0.00015% (w/v) CHS, and further purified by a Superose 6 column (Cytiva) using a buffer containing 20 mM HEPES 7.5, 150 mM NaCl, 10 mM $CaCl_2$, 40 μM L-Trp, 50 μM compound and 0.00075% (w/v) LMNG, 0.00025% (w/v) GDN and 0.00015% (w/v) CHS. The peak fractions were pooled and concentrated for cryo-EM studies.

`

Cryo-EM data acquisition and data processing

For cryo-EM imaging of the CaSR-'6218 complex, movies were collected using a Titan Krios G2 (Thermo Fisher Scientific) transmission electron microscope equipped with a Gatan K3 direct detector and a post-column energy filter with a 20 eV slit width. The microscope was operated at 300 kV, with a nominal magnification of 130,000x, resulting in a pixel size of 0.8677 Å. Movies were automatically recorded in counting mode using SerialEM[51] with a total exposure of 55 electrons·$Å^{-2}$ over 60 frames, and the defocus range was set from -0.5 to -1.5 µm. For cryo-EM imaging of the CaSR-'54159 complex, movies were collected using a Titan Krios G2 transmission electron microscope equipped with a Falcon 4i Direct Electron Detector and a post-column energy filter with a 20 eV slit width. The microscope was operated at 300 kV, with a nominal magnification of 165,000x, resulting in a pixel size of 0.75 Å. Movies were recorded in counting mode using EPU 3.6 (Thermo Fisher Scientific) with a total exposure of 50 electrons·$Å^{-2}$ over 50 frames, and the defocus range was set from -0.5 to -1.5 µm.

For a detailed workflow of data processing, please refer to Extended Data Fig. 4. All data underwent processing using similar strategies using cryoSPARC 3.0[52] and Relion 3[53]. Movies were imported into cryoSPARC and subjected to patch motion correction, followed by the contrast transfer function (CTF) estimation using patch CTF estimation. Micrographs with CTF estimations worse than 4 Å were excluded, resulting in a total of 11,926 micrographs for the CaSR-‘6218 complex, and 17,625 micrographs for the CaSR-‘54149 complexes, which were selected for further processing. Particles were autopicked, extracted from the micrographs, and subjected to 3-5 rounds of 2D classification. Particles classified into “good” classes were selected and subjected to iterative rounds of 3D ab initio reconstruction using multiple classes, followed by 3D heterogeneous refinement to remove particles from bad classes. For the early rounds of 3D classification, particles from “bad” classes were further classified by 2D classification and good particles were retained for subsequent heterogeneous refinement. The resulting high-quality particle projections were then imported into Relion, where they were subjected to C2 symmetry

`

expansion, followed by 2-3 rounds of focused 3D classification (without applying symmetry) without alignment with a mask covering the two 7TMs of CaSR. Finally, the particles from one of the two best 3D classes with C1 symmetry were selected and imported to cryoSPARC for CTF refinement and local nonuniform refinement with a soft mask covering CRD–7TM and ECD-CRD to obtain high-resolution maps. The focused maps were used to generate composite maps for refinement.

Model building and refinement

The initial models of CaSR were built on the structure of the active-state CaSR (PDB ID: 7M3F) and manually docked into the cryo-EM maps in Chimera[54]. The models were then subjected to iterative rounds of manual refinement in Coot[55] and automatic real-space refinement in Phenix[56]. The models for CRD–7TM and ECD-CRD regions were refined using the focused maps that cover these regions first and then combined for further refinement using the composite maps. The final models were analyzed and validated using MolProbity[57]. The refinement statistics are shown in Extended Data Table 2. Structure figures were generated using ChimeraX[58].

Animal studies

Pharmacokinetics (PK) studies were performed on 10-weekold male CD1 mice by BIENTA Enamine Biology Services (Kiev, Ukraine). Briefly, the animals were randomly assigned to treatment groups for 9 time points (5, 15, 30, 60, 120, 240, 360, 480, and 1440 min) and fasted for 4 h before dosing with each PAM by subcutaneous (SC) route. At each time point post-injection, mice were injected IP with 2,2,2-tribromoethanol at the dose of 150 mg/kg prior to blood draws. All other animal studied were performed on 12-16 weeks old male C57/B6 mice (Jackson Laboratory; Bar Harbor, Maine, USA), approved by the Institutional Animal Care and Use Committee of the San Francisco Department of Veteran Affairs Medical Center (Protocol numbers: 2021–005 and 2021–016). For the latter studies, test compounds with specified doses were

injected subcutaneously for 6 different time points (15, 30, 60, 120, 240, and 480 min), followed by isoflurane overdose before blood collections by cardiac puncture. Sera were prepared by centrifugation (2000xg) in microtainer (Becton Dickinson, SST 365967) and assayed for PTH levels by ELISA (Quidel, 60-2305) and total calcium using Alfa Wassermann ACE Axcel Vet Chemistry Analyzer.

Ex vivo parathyroid gland culture

Mouse PTGs were isolated from 4-week-old male C57/B6 mice, dissected free of thyroid and surrounding fibrous tissues, and cultured to assess PTH secretion rate (ng/gland/hr) and Ca^{2+} set-point ($[Ca^{2+}]_e$ needed to suppress 50% of PTH_{max})[59,60]. Briefly, PTGs were incubated sequentially with a series of DMEM media containing increasing concentrations of PAM at 0.75 mM calcium or containing increasing $[Ca^{2+}]_e$ with (50 or 500 nM) or without PAM to be tested. Intact PTH levels in culture media were assessed by ELISA and use to calculate the EC_{50} or Ca^{2+} set-points for each PAM.

References

1 Brown, E. M. *et al.* Cloning and characterization of an extracellular Ca(2+)-sensing receptor from bovine parathyroid. *Nature* **366**, 575-580, doi:10.1038/366575a0 (1993).

2 Leach, K. *et al.* International Union of Basic and Clinical Pharmacology. CVIII. Calcium-Sensing Receptor Nomenclature, Pharmacology, and Function. *Pharmacol Rev* **72**, 558-604, doi:10.1124/pr.119.018531 (2020).

3 Hannan, F. M., Kallay, E., Chang, W., Brandi, M. L. & Thakker, R. V. The calcium-sensing receptor in physiology and in calcitropic and noncalcitropic diseases. *Nat Rev Endocrinol* **15**, 33-51, doi:10.1038/s41574-018-0115-0 (2018).

4 Hannan, F. M. & Thakker, R. V. Calcium-sensing receptor (CaSR) mutations and disorders of calcium, electrolyte and water metabolism. *Best Pract Res Clin Endocrinol Metab* **27**, 359-371, doi:10.1016/j.beem.2013.04.007 (2013).

5 Pollak, M. R. *et al.* Autosomal dominant hypocalcaemia caused by a Ca(2+)-sensing receptor gene mutation. *Nat Genet* **8**, 303-307, doi:10.1038/ng1194-303 (1994).

6 Hannan, F. M. *et al.* Identification of 70 calcium-sensing receptor mutations in hyper- and hypo-calcaemic patients: evidence for clustering of extracellular domain mutations at calcium-binding sites. *Hum Mol Genet* **21**, 2768-2778, doi:10.1093/hmg/dds105 (2012).

7 Pearce, S. H. *et al.* A familial syndrome of hypocalcemia with hypercalciuria due to mutations in the calcium-sensing receptor. *N Engl J Med* **335**, 1115-1122, doi:10.1056/NEJM199610103351505 (1996).

`

8 Patel, J. & Bridgeman, M. B. Etelcalcetide (Parsabiv) for Secondary Hyperparathyroidism in Adults With Chronic Kidney Disease on Hemodialysis. *P T* **43**, 396-399 (2018).

9 Sauter, T. C. *et al.* Calcium Disorders in the Emergency Department: Independent Risk Factors for Mortality. *PLoS One* **10**, e0132788, doi:10.1371/journal.pone.0132788 (2015).

10 Zhang, Z., Xu, X., Ni, H. & Deng, H. Predictive value of ionized calcium in critically ill patients: an analysis of a large clinical database MIMIC II. *PLoS One* **9**, e95204, doi:10.1371/journal.pone.0095204 (2014).

11 Egi, M. *et al.* Ionized calcium concentration and outcome in critical illness. *Crit Care Med* **39**, 314-321, doi:10.1097/CCM.0b013e3181ffe23e (2011).

12 Steele, T., Kolamunnage-Dona, R., Downey, C., Toh, C. H. & Welters, I. Assessment and clinical course of hypocalcemia in critical illness. *Crit Care* **17**, R106, doi:10.1186/cc12756 (2013).

13 Husain, A., Simpson, R. J., Jr. & Joodi, G. Serum Calcium and Risk of Sudden Cardiac Arrest in the General Population. *Mayo Clin Proc* **93**, 392, doi:10.1016/j.mayocp.2017.12.022 (2018).

14 Nardone, R., Brigo, F. & Trinka, E. Acute Symptomatic Seizures Caused by Electrolyte Disturbances. *J Clin Neurol* **12**, 21-33, doi:10.3988/jcn.2016.12.1.21 (2016).

15 Pin, J. P., Galvez, T. & Prezeau, L. Evolution, structure, and activation mechanism of family 3/C G-protein-coupled receptors. *Pharmacol Ther* **98**, 325-354, doi:10.1016/s0163-7258(03)00038-x (2003).

16 Gao, Y. *et al.* Asymmetric activation of the calcium-sensing receptor homodimer. *Nature* **595**, 455-459, doi:10.1038/s41586-021-03691-0 (2021).

17 Seven, A. B. *et al.* G-protein activation by a metabotropic glutamate receptor. *Nature* **595**, 450-454, doi:10.1038/s41586-021-03680-3 (2021).

18 Papasergi-Scott, M. M. *et al.* Structures of metabotropic GABA(B) receptor. *Nature* **584**, 310-314, doi:10.1038/s41586-020-2469-4 (2020).

19 Lyu, J. *et al.* Ultra-large library docking for discovering new chemotypes. *Nature* **566**, 224-229, doi:10.1038/s41586-019-0917-9 (2019).

20 Gorgulla, C. *et al.* An open-source drug discovery platform enables ultra-large virtual screens. *Nature* **580**, 663-668, doi:10.1038/s41586-020-2117-z (2020).

21 Stein, R. M. *et al.* Virtual discovery of melatonin receptor ligands to modulate circadian rhythms. *Nature* **579**, 609-614, doi:10.1038/s41586-020-2027-0 (2020).

22 Alon, A. *et al.* Structures of the sigma(2) receptor enable docking for bioactive ligand discovery. *Nature* **600**, 759-764, doi:10.1038/s41586-021-04175-x (2021).

23 Sadybekov, A. A. *et al.* Synthon-based ligand discovery in virtual libraries of over 11 billion compounds. *Nature* **601**, 452-459, doi:10.1038/s41586-021-04220-9 (2022).

24 Fink, E. A. *et al.* Structure-based discovery of nonopioid analgesics acting through the alpha(2A)-adrenergic receptor. *Science* **377**, eabn7065, doi:10.1126/science.abn7065 (2022).

25 Singh, I. *et al.* Structure-based discovery of conformationally selective inhibitors of the serotonin transporter. *Cell* **186**, 2160-2175 e2117, doi:10.1016/j.cell.2023.04.010 (2023).

26 Coleman, R. G., Carchia, M., Sterling, T., Irwin, J. J. & Shoichet, B. K. Ligand pose and orientational sampling in molecular docking. *PLoS One* **8**, e75992, doi:10.1371/journal.pone.0075992 (2013).

27 Meng, E. C., Shoichet, B. K. & Kuntz, I. D. Automated Docking with Grid-Based Energy Evaluation. *J Comput Chem* **13**, 505-524, doi:DOI 10.1002/jcc.540130412 (1992).

28 Sharp, K. A., Friedman, R. A., Misra, V., Hecht, J. & Honig, B. Salt effects on polyelectrolyte-ligand binding: comparison of Poisson-Boltzmann, and limiting law/counterion binding models. *Biopolymers* **36**, 245-262, doi:10.1002/bip.360360211 (1995).

`

29 Gallagher, K. & Sharp, K. Electrostatic contributions to heat capacity changes of DNA-ligand binding. *Biophys J* **75**, 769-776, doi:10.1016/S0006-3495(98)77566-6 (1998).

30 Mysinger, M. M. & Shoichet, B. K. Rapid context-dependent ligand desolvation in molecular docking. *J Chem Inf Model* **50**, 1561-1573, doi:10.1021/ci100214a (2010).

31 Gu, S., Smith, M. S., Yang, Y., Irwin, J. J. & Shoichet, B. K. Ligand Strain Energy in Large Library Docking. *J Chem Inf Model* **61**, 4331-4341, doi:10.1021/acs.jcim.1c00368 (2021).

32 Olsen, R. H. J. *et al.* TRUPATH, an open-source biosensor platform for interrogating the GPCR transducerome. *Nat Chem Biol* **16**, 841-849, doi:10.1038/s41589-020-0535-8 (2020).

33 Tingle, B. I. *et al.* ZINC-22 horizontal line A Free Multi-Billion-Scale Database of Tangible Compounds for Ligand Discovery. *J Chem Inf Model* **63**, 1166-1176, doi:10.1021/acs.jcim.2c01253 (2023).

34 Lyu, J., Irwin, J. J. & Shoichet, B. K. Modeling the expansion of virtual screening libraries. *Nat Chem Biol* **19**, 712-718, doi:10.1038/s41589-022-01234-w (2023).

35 Leach, K. *et al.* Towards a structural understanding of allosteric drugs at the human calcium-sensing receptor. *Cell Res* **26**, 574-592, doi:10.1038/cr.2016.36 (2016).

36 Keller, A. N. *et al.* Identification of Global and Ligand-Specific Calcium Sensing Receptor Activation Mechanisms. *Mol Pharmacol* **93**, 619-630, doi:10.1124/mol.118.112086 (2018).

37 Lin, S. *et al.* Structures of G(i)-bound metabotropic glutamate receptors mGlu2 and mGlu4. *Nature* **594**, 583-588, doi:10.1038/s41586-021-03495-2 (2021).

38 Brown, E. M. Clinical lessons from the calcium-sensing receptor. *Nat Clin Pract Endocrinol Metab* **3**, 122-133, doi:10.1038/ncpendmet0388 (2007).

39 Block, G. A. *et al.* Effect of Etelcalcetide vs Cinacalcet on Serum Parathyroid Hormone in Patients Receiving Hemodialysis With Secondary Hyperparathyroidism: A Randomized Clinical Trial. *JAMA* **317**, 156-164, doi:10.1001/jama.2016.19468 (2017).

40 Jamal, S. A. & Miller, P. D. Secondary and tertiary hyperparathyroidism. *J Clin Densitom* **16**, 64-68, doi:10.1016/j.jocd.2012.11.012 (2013).

41 Rodriguez, M., Nemeth, E. & Martin, D. The calcium-sensing receptor: a key factor in the pathogenesis of secondary hyperparathyroidism. *Am J Physiol Renal Physiol* **288**, F253-264, doi:10.1152/ajprenal.00302.2004 (2005).

42 Centeno, P. P. *et al.* Phosphate acts directly on the calcium-sensing receptor to stimulate parathyroid hormone secretion. *Nat Commun* **10**, 4693, doi:10.1038/s41467-019-12399-9 (2019).

43 Gogusev, J. *et al.* Depressed expression of calcium receptor in parathyroid gland tissue of patients with hyperparathyroidism. *Kidney Int* **51**, 328-336, doi:10.1038/ki.1997.41 (1997).

44 Schmidt, G. S., Weaver, T. D., Hoang, T. D. & Shakir, M. K. M. Severe Symptomatic Hypocalcemia, complicating cardiac arrhythmia following Cinacalcet (Sensipar(TM)) administration: A Case Report. *Clin Case Rep* **9**, e04876, doi:10.1002/ccr3.4876 (2021).

45 Block, G. A. *et al.* Cinacalcet for secondary hyperparathyroidism in patients receiving hemodialysis. *N Engl J Med* **350**, 1516-1525, doi:10.1056/NEJMoa031633 (2004).

46 Word, J. M., Lovell, S. C., Richardson, J. S. & Richardson, D. C. Asparagine and glutamine: using hydrogen atom contacts in the choice of side-chain amide orientation. *J Mol Biol* **285**, 1735-1747, doi:10.1006/jmbi.1998.2401 (1999).

47 Sastry, G. M., Adzhigirey, M., Day, T., Annabhimoju, R. & Sherman, W. Protein and ligand preparation: parameters, protocols, and influence on virtual screening enrichments. *J Comput Aided Mol Des* **27**, 221-234, doi:10.1007/s10822-013-9644-8 (2013).

48 Sharp, K. A. Polyelectrolyte Electrostatics - Salt Dependence, Entropic, and Enthalpic Contributions to Free-Energy in the Nonlinear Poisson-Boltzmann Model. *Biopolymers* **36**, 227-243, doi:DOI 10.1002/bip.360360210 (1995).

`

49 Stein, R. M. *et al.* Property-Unmatched Decoys in Docking Benchmarks. *J Chem Inf Model* **61**, 699-714, doi:10.1021/acs.jcim.0c00598 (2021).

50 Fassio, A. V. *et al.* Prioritizing Virtual Screening with Interpretable Interaction Fingerprints. *J Chem Inf Model* **62**, 4300-4318, doi:10.1021/acs.jcim.2c00695 (2022).

51 Mastronarde, D. N. Automated electron microscope tomography using robust prediction of specimen movements. *J Struct Biol* **152**, 36-51, doi:10.1016/j.jsb.2005.07.007 (2005).

52 Punjani, A., Rubinstein, J. L., Fleet, D. J. & Brubaker, M. A. cryoSPARC: algorithms for rapid unsupervised cryo-EM structure determination. *Nat Methods* **14**, 290-296, doi:10.1038/nmeth.4169 (2017).

53 Zivanov, J. *et al.* New tools for automated high-resolution cryo-EM structure determination in RELION-3. *Elife* **7**, doi:10.7554/eLife.42166 (2018).

54 Pettersen, E. F. *et al.* UCSF Chimera--a visualization system for exploratory research and analysis. *J Comput Chem* **25**, 1605-1612, doi:10.1002/jcc.20084 (2004).

55 Emsley, P., Lohkamp, B., Scott, W. G. & Cowtan, K. Features and development of Coot. *Acta Crystallogr D Biol Crystallogr* **66**, 486-501, doi:10.1107/S0907444910007493 (2010).

56 Liebschner, D. *et al.* Macromolecular structure determination using X-rays, neutrons and electrons: recent developments in Phenix. *Acta Crystallogr D Struct Biol* **75**, 861-877, doi:10.1107/S2059798319011471 (2019).

57 Chen, V. B. *et al.* MolProbity: all-atom structure validation for macromolecular crystallography. *Acta Crystallogr D Biol Crystallogr* **66**, 12-21, doi:10.1107/S0907444909042073 (2010).

58 Pettersen, E. F. *et al.* UCSF ChimeraX: Structure visualization for researchers, educators, and developers. *Protein Sci* **30**, 70-82, doi:10.1002/pro.3943 (2021).

59 Chang, W., Tu, C., Chen, T. H., Bikle, D. & Shoback, D. The extracellular calcium-sensing receptor (CaSR) is a critical modulator of skeletal development. *Sci Signal* **1**, ra1, doi:10.1126/scisignal.1159945 (2008).

60 Chang, W. *et al.* PTH hypersecretion triggered by a GABA(B1) and Ca(2+)-sensing receptor heterocomplex in hyperparathyroidism. *Nat Metab* **2**, 243-255, doi:10.1038/s42255-020-0175-z (2020).